2012 IEEE International Conference on Robotics and Automation
RiverCentre, Saint Paul, Minnesota, USA
May 14-18, 2012

Three-dimensional control of engineered motile cellular microrobots

Dal Hyung Kim*, Paul Seung Soo Kim*, Anak Agung Julius† and Min Jun Kim*

Abstract— **We demonstrate three-dimensional control with the eukaryotic cell *Tetrahymena pyriformis* (*T. pyriformis*) using two sets of Helmholtz coils for *xy*-plane motion and a single electromagnet for vertical motion. *T. pyriformis* is modified to have artificial magnetotaxis with internalized magnetite. Since the magnetic fields exerted by electromagnets are relatively uniform in the working space, the magnetite exerts only torque, without translational force, which enabled us to guide the cell's swimming direction while the swimming force is exerted only by the cell's motile organelles. A stronger magnetic force was necessary to steer cells to the *z*-axis, and, as a result, a single electromagnet placed just below our sample area is utilized for vertical motion. To track the cell's positions in the *z*-axis, intensity profiles of non-motile cells at varying distances from the focal plane are used. During vertical motion along the *z*-axis, the intensity difference from the background decreases while the cell size increases. Since the cell is pear-shaped, the eccentricity is high during planar motion, but lowers during vertical motion due to the change in orientation. The three-dimensional control of the live organism *T. pyriformis* as a cellular robot shows great potential to be utilized for practical applications in microscale tasks, such as target transport and cell therapy.**

Keywords: *Tetrahymena pyriformis*, Artificial magnetotaxis, Three-dimensional control, Microrobot

I. INTRODUCTION

Developing microrobots for low Reynolds number environment entails developing swimming systems that can overcome the viscous forces. Nature has already developed these swimming mechanisms, such as flagella and cilia, and researchers have already investigated imitating these motile organelles for use in microrobotics [1]–[4]. One of the biggest hurdles for artificial microrobots is developing onboard power sources, which is why microorganisms' established propulsion systems that overcome the dominant viscous forces are good candidates for use in microrobotics. We have been able to harness *Tetrahymena pyriformis* (*T. pyriformis*) as a microrobot by using magnetotaxis to steer the cells [5].

We have previously demonstrated two-dimensional (2D) tracking of *T. pyriformis* [6]. The transition from 2D tracking to three-dimensional (3D) tracking requires much more of a complex imaging system. Tracking microorganisms in 3D started in the 1970s; a complex feedback system was created to keep a single bacterium in focus [7]. More developed systems utilize two imaging devices [8, 9], with each focused on a different plane (*xz*, *yz*, and/or *xy*). By combining synced images of both planes, 3D trajectories can be calculated. Different methods can also be found when looking at 3D tracking of particles; pyramidal micromirrors wells are utilized to track fluorescent particles using the projected reflections to determine the particle's motion [10].

In this paper, 3D control of artificial *T. pyriformis* is accomplished through a multifunctional approximate Helmholtz coil system. To determine the cell's position in the *z*-axis, intensity profiles of deciliated cells are obtained at different depths. We used an open loop control system to steer *T. pyriformis* and then used the predetermined intensity profile to calculate the cell's trajectory. The successful application of 3D control and tracking furthers *T. pyriformis*' use as a microbiorobot.

II. ARTIFICIAL MAGNETOTACTIC *T. PYRIFORMIS*

A. Synthesis of artificial magnetotactic T. pyriformis

T. pyriformis is cultured in 0.1% (w/v) select yeast extract (Sigma Aldrich, MO, USA) and 1% (w/v) tryptone (Sigma Aldrich) in deionized water. Cell cultures are maintained at 28 °C in an incubator. Cell lines are maintained by inoculating cells weekly with new culture medium at a ratio of 1:10. Newly inoculated cells typically reach full saturation in 48 hours [11]. The average cell size of *T. pyriformis*, Figure 1 (a), is 25 μm by 50 μm. Its entire cell body is covered with approximately 600 cilia, consisting of both motile and oral cilia [12].

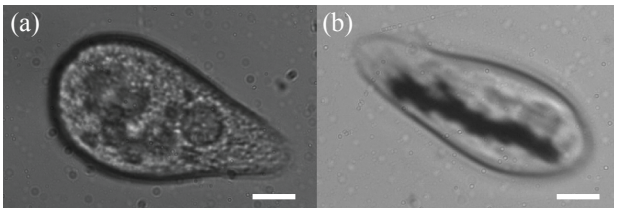

Fig. 1. (a) Normal *T. pyriformis* cell. (b) *T. pyriformis* with ingested magnetite in a magnetic field. The scale bar is 10μm.

To create artificial magnetotactic *T. pyriformis*, 50 *nm* diameter iron-oxide particles (Sigma Aldrich) are introduced into a sample of cells in culture medium. The cells ingest the particles through their oral apparatus located at the anterior and enclose them in vesicles. *T. pyriformis* can consume particles up to 2.7 μm in diameter [13]. To ensure uptake of the particles, mixed samples are left for 10 minutes. Magnetization of the particles is accomplished by applying a neodymium-iron-boron magnet (K&J Magnetics, Inc., PA, USA) with a surface field of 1964 Gauss to the sample

*Department of Mechanical Engineering and Mechanics, Drexel University, Philadelphia, PA 19104, USA Dalhyung.Kim, paul.s.kim@drexel.edu, mkim@coe.drexel.edu,
†Department of Electrical, Computer and Systems Engineering, Rensselaer Polytechnic Institute, Troy, NY 12180, USA agung@ecse.rpi.edu

for 1 minute; this ensures magnetization of the magnetite. After exposure to the magnet, the magnetite retains its dipole strength for at least an hour; thus, it is assumed that the dipole strength is constant during experiments [6]. Figure 1 (b) shows artificial magnetotactic *T. pyriformis* when exposed to a magnetic field.

To obtain the intensity profiles of *T. pyriformis* for 3D cell tracking, images of stationary cells were taken at uniformly varying depths, usually in 10 μm increments, moving the objective further away from the cell. To prevent the cells from moving and obtain accurate intensity profiles, a deciliation process [14] was used. 0.5 mM dibucaine HCl (Sigma Aldrich) is introduced to *T. pyriformis* culture at a ratio of 1:9. After 4 minutes, new culture medium is added to the sample at a ratio of 20:1. Under- or overexposing the cells results in many cells still able to swim or dead cells with abnormal shapes, respectively. The sample is then centrifuged at 370g for 5 minutes and a small amount of the sample is taken from the bottom of the centrifuge tube where the cell concentration is high. Cells, otherwise, are difficult to obtain because of the large addition of new culture medium. The deciliated cells are then analyzed for their intensity profiles at varying depths.

B. Magnetization of artificial magnetotactic T. pyriformis

The iron oxide particles ingested by *T. pyriformis* are ferromagnetic. Due to the nature of ferromagnetism, the magnetic momentum of the magnetite should be fully saturated to react with magnetic fields. Figure 2 (a) is the hysteresis graph, which shows the relationship between the applied magnetic fields and the magnetic momentum of the iron oxide particles. The magnetic momentum of iron oxide particles are fully saturated when a magnetic field of about 111.5 mT is applied. Thus, a permanent magnet with surface field strength of 1964 Gauss is utilized for magnetization. The torque applied by the internalized iron oxide particles is computed based on the equation (1) [15].

$$\tau = \mathbf{m} \times \mathbf{B} = mB \sin\theta \tag{1}$$

where τ, $\mathbf{m}$, $\mathbf{B}$ and θ are torque, magnetic moment, the magnetic fields and the angle between $\mathbf{m}$ and $\mathbf{B}$, respectively. Since the magnetic moment $\mathbf{m}$, after saturation, and the strength of the magnetic field $\mathbf{B}$ are constant, the torque is determined by the angle θ. When there is an angle θ, shown in Figure 2 (b), the torque exerted by the iron oxide particles tends to align the cell with the magnetic field. Once a cell is aligned, shown in Figure 2 (c), the cell swims along the magnetic fields while the iron oxide particles do not create any torque.

III. CONTROL AND LOCALIZATION IN THREE-DIMENSIONAL SPACE

A. Magnetic control system

The system used is illustrated in Figure 3 (a). Two sets of approximate Helmholtz coils are used for x and y axes, and one electromagnetic coil is utilized for z-axis control.

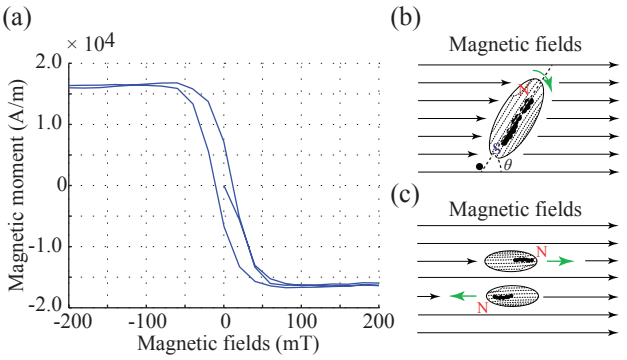

Fig. 2. (a) Hysteresis graph of iron oxide particles. The magnetic moment of iron oxide particles is saturated when magnetic fields of about 111.5 mT are applied. Observation starts with non-magnetized iron oxide particles so the curve starts at zero for both the magnetic field and magnetic moment. (b) The cell's reaction when cell's swimming direction and magnetic fields are not aligned and (c) when they are aligned.

The coil frame is set on an inverted microscope (Leica DM IRB) and the images are captured at 10 frames per second using a high resolution camera (MotionPro X3). A computer calculates the positions of the cells using the captured images. The power supply is controlled manually through software. In Figure 3 (b), both the top and bottom

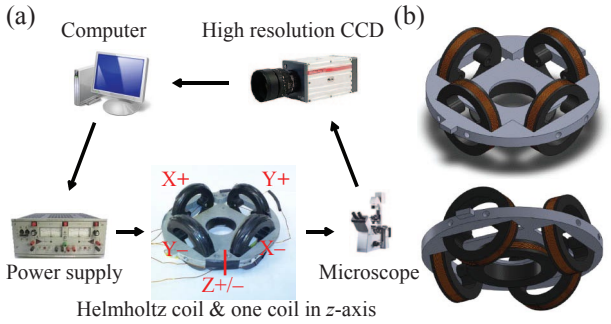

Fig. 3. The 3D magnetic control system for artificial magnetotactic *T. pyriformis*. (a) System drawing and (b) coil configuration drawing in two different views.

of the coil configuration are illustrated. The approximate Helmholtz coils are designed to generate uniform magnetic fields of about 2.5 mT to exert a torque without translational force. Using the combination of magnetic fields exerted by the two sets of Helmholtz coils in the x and y axes, the directional control of the magnetic fields is achieved. One electromagnet for z-axis control is located on the bottom of the stage illustrated in Figure 3 (b). We found that a stronger magnetic field is needed to steer a cell to the z-axis. This may be attributed to gravity, but further investigation is still necessary. Thus, instead using a Helmholtz coil configuration for z-axis control, we utilized one electromagnet close to the sample area.

Figure 4 (a) shows the simulation results of the magnetic fields created along the x-axis. Since the field of view of the microscope is small at 2×3 mm^2, the gradient of the magnetic fields is negligible from -3 mm to 3 mm in

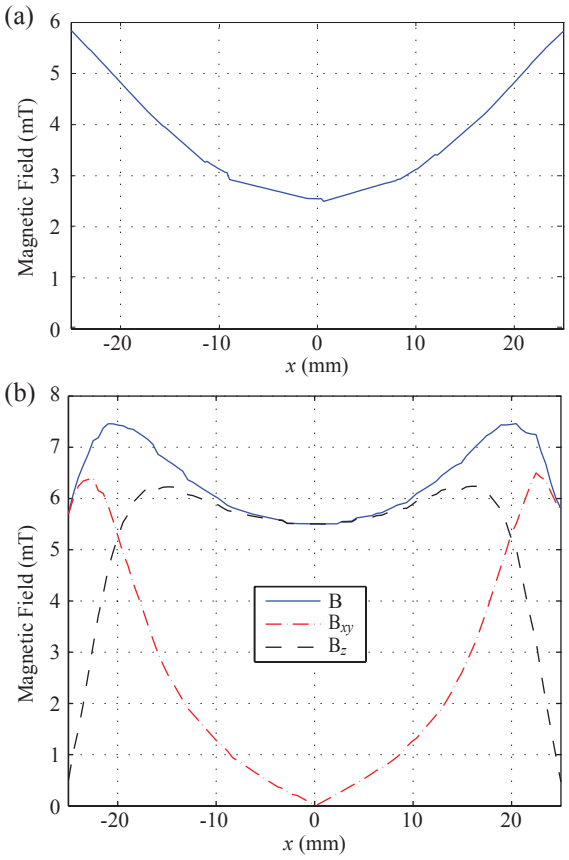

Fig. 4. Simulation result of the strength of the magnetic field. (a) In the case that the one set of Helmholtz coil is activated, the strength of magnetic fields is about 2.5 mT at the center. (b) When one electromagnet in the z-axis is activated, the strength is about 5.5 mT at the center (B or B_z), while that of xy-plane (B_{xy}) is negligible. B, B_{xy}, B_z is the strength of the entire, xy component, and z-axis component of the magnetic field, respectively.

Figure 4 (a). Thus, we assumed only torque is exerted by the internalized magnetite. In Figure 4 (b), the simulation results show there are only magnetic fields along the z-axis with strength of about 5.5 mT, which is also relatively uniform at the center, while the x and y components of the fields are negligible. Because of our small field of view, we assumed that a uniform magnetic field along the z-axis is generated without any magnetic fields in xy-plane. The control of artificial magnetotactic *T. pyriformis* in 3D is achieved by manipulating these coils. Two sets of Helmholtz coils are manipulated to control a cell in the xy-plane, and one electromagnet located on the bottom is utilized to control a cell to travel along the z-axis.

B. Localization of T. pyriformis in three-dimensional space

The major challenge of microscale 3D tracking is that only the focal plane is available for observation when using the microscope, in most cases. 3D tracking of microspheres has been studied widely because the z-axis position is able to be accurately calculated with its Gaussian distributed intensity profile created by its spherical shape [16]. When a microsphere is far from the focal plane, the distribution becomes wider and the maximum intensity decreases, with either property unaffected by the microsphere's orientation.

However, 3D tracking of microorganisms and determining the z-axis position are difficult, due to the deformation and uneven intensity profile of a cell. In most cases, the cell does not have a perfect sphere shape and its intensity profile is different from a Gaussian distribution because the intensity inside of the cell is similar with the background while that of the membrane differs. Normally, the intensity distribution of the cells has two peaks in the cross section, with each peak corresponding to the membrane on either side of the cell. When a cell is far from the focal plane, the image is blurred, resulting in a decrease of the maximum intensity and a widening of the intensity distribution. Thus, the two peaks are hard to recognize and blend together. At a long distance from the focal plane, the intensity of the cell and that of the background became indiscernible.

The intensity information of the cell is used to estimate the z-axis position. Typically, the maximum intensity and distribution is used to determine the z-axis position. However, for our experiments, a mean intensity difference between the cell and the background is used because it is quite consistent among cells. The intensity of the cell is determined by the average intensity of the pixels occupied by the cell, while that of the background is determined by the immediate unoccupied area around the cell.

To understand the relationship between the mean intensity difference and a cell's position in z-axis, non-motile *T. pyriformis* were prepared and observed under the microscope while changing the focal plane. Non-motile *T. pyriformis* was obtained through a deciliation process [14] described in Section II-B. When deciliated cells are placed on the glass slide, most of the cells settle on the bottom because they lost their motility. The microscope is then focused on the settled cells. The intensity of the cells was observed under the microscope while the position in the z direction is manipulated manually. Even though both dead and deciliated cells are not motile, the shape of dead *T. pyriformis* is characterized by a circular shape [17], while that of a normal, nondeciliated cell is pear-shaped. To obtain intensity information similar to that of motile cells, which are also pear-shaped, the intensity profile of deciliated cells are used.

Figure 5 shows the mean intensity difference between a cell and the background versus the z-axis position. Ten cells have been observed from 0 to 500 μm in the z-axis, where 0 μm is defined as a cell in focus, and a positive value denotes an increase in distance between the original focal plane (0 μm) and the objective. Circle and cross markers represent the first region from 0 to 20 μm and the second region beyond 20 μm, respectively. Each marker represents a captured image of the cell; there are about 300 markers total. From 0 to 20 μm in the z-axis, the mean intensity difference increases; beyond 20 μm, it decreases exponentially. Thus, curve fitting was separately conducted for each region. One data set from 0 to 20 μm in the z-axis was fitted with the linear curve, whose slope is 1.375 μm^{-1}. The other data set from 20 to 500 μm in the z-axis was fitted with the exponential equation

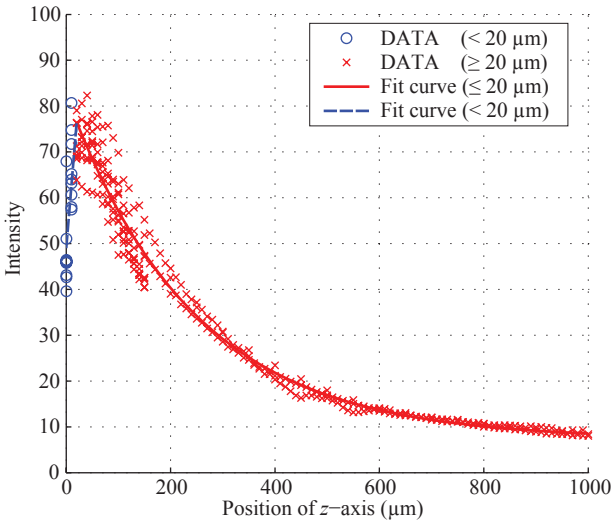

Fig. 5. The intensity difference between *T. pyriformis* and the background from 0 to 500 μm. From 0 to 20 μm, the intensity difference increases and the data are fitted with a linear curve. From 20 to 500 μm, it decreases exponentially and the data is fitted using Equation (2).

expressed as follows.

$$I = ae^{-bz} + c, \tag{2}$$

where I is the mean intensity difference and z is the position in z-axis. The parameters a, b and c are 75.13, 0.004 and 7.316, respectively. When the position in the z-axis is 20 μm, the mean intensity difference has a maximum value of 76.51. *T. pyriformis* normally swim above the substrate and when they are located close to the substrate's surface, their swimming speed decreases, a case in which we are not interested. Thus, we assumed that the cell swims 20 μm above the substrate which is focused as a datum. The position in z-axis is estimated by the equation (2).

IV. RESULTS AND DISCUSSION

Magnetotactic *T. pyriformis* are controlled manually in three dimensions. The cell's motion was controlled in two different modes: one mode is planar in the xy-plane and the other is vertical on the z-axis. Planar motion was conducted by only the Helmholtz coils while the z-axis coil was off. Vertical motion was achieved using only the z-axis coil. Magnetotactic *T. pyriformis* were prepared on the substrate in an open channel to ensure sufficient depth for the cell to swim. Figure 6 (a)-(l) shows the sequence images of the manually controlled *T. pyriformis* and the lines and circle markers are the trajectories and centroids, respectively. The cell's trajectory can be seen in Figure 6 (m), where the planar mode of motion occurs in two distinct xy-planes. The xy-planes that are about 127.0 μm and 446.6 μm above the focal plane can be referred to as the lower plane and upper plane, respectively. In Figure 6 (a), *T. pyriformis* was controlled in planar mode in the lower plane, while their position in the z-axis was maintained. To steer the cell along the z-axis, electromagnets in the x and y axes were turned off and

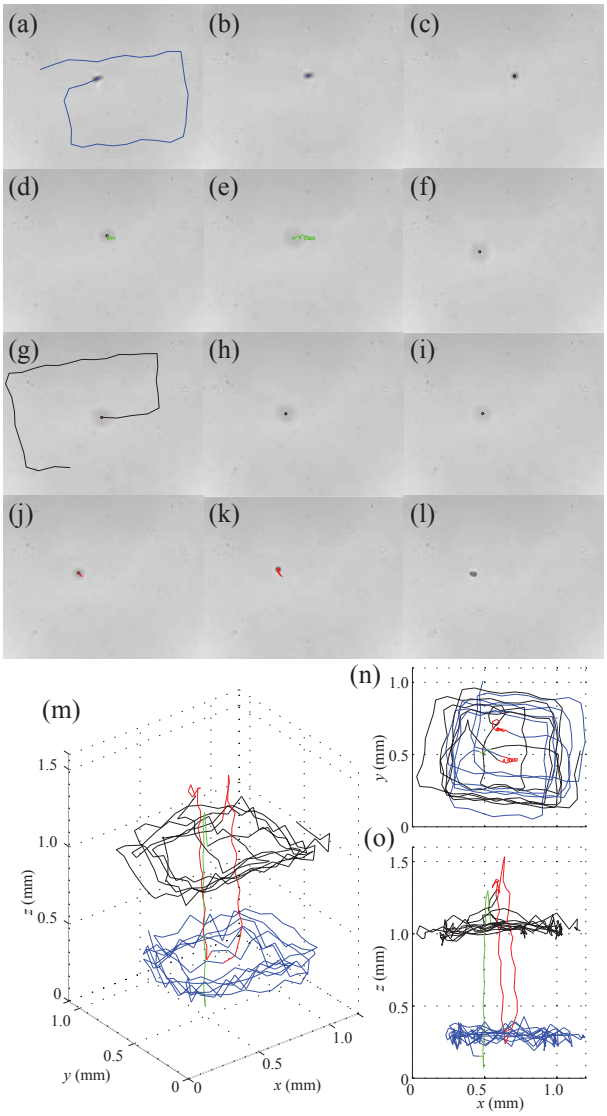

Fig. 6. The manual control experiment. (a)-(l) The sequence of images of (a) planar motion at around 127.0 μm from the focal plane, (b)-(f) upward vertical motion, (g) planar motion at around 446.6 μm from the focal plane, and (h)-(l) downward vertical motion. The scale bar is 100 μm. (m) The trajectory in a 3D view, (n) a view of xy-plane and (o) xz-plane. The blue and black lines represent the trajectories in the lower plane and the upper plane, respectively. The green and red lines represent the trajectories in the z-axis for upwards and downwards motion, respectively.

only the electromagnet in the z-axis was activated to create a magnetic field on the z-axis. Figure 6 (b)-(f) are the series of pictures when the cell swims from the lower to the upper plane. As shown in Figure 6 (b), magnetotactic *T. pyriformis* is still pear-shaped when swimming in the lower plane while in planar mode. As shown in Figure 6 (c), the cell's shape became circular when the electromagnet in only the z-axis is activated. When a cell aligns with the magnetic field in the z-axis, its anterior is pointed at the positive or negative direction in the z-axis, depending on its polarity, resulting in what appears to be a circular cell shape. Figure 6 (d)-(e) shows the cell and its trajectory when it moves along the z-axis. When the cell moves upward, the intensity difference

between the cell and the background decreased and the cell size increased. The helical trajectory indicates that the cell swims with a corkscrew motion. In Figure 6 (f), the cell's motion was switched to planar mode in the upper plane. At this depth, the cell appears to be an amorphous blur. Figure 6 (g) shows the trajectory of the magnetotactic *T. pyriformis* controlled by magnetic field in the x and y axes on the upper plane. The intensity difference of the cell is still recognizable but its difference is not significant.

From Figure 6 (h)-(k), downward movement in the z-axis is illustrated. Figure 6 (h) and (i) are the images before and after the magnetic field in the z-axis is applied, respectively. Since the cell is located far from the focal plane, it is hard to observe the change of its shape like that in Figure 6 (b) and (c). The downward swimming is illustrated in Figure 6 (i)-(k) and the corkscrew motion is also observable; it is has a coil like trajectory. The cells became distinct from the background and their intensity difference increased. Figure 6 (l) shows the motion in the lower plane after travelling along the z-axis. The cell shape changed to its original pear-shape because it is close to the focal plane.

The whole trajectory for about 40 seconds is illustrated in three-dimensional space in Figure 6 (m). Figure 6 (n) and (o) represent the same trajectory in the xy and xz planes, respectively. There are peaks on the trajectory in the z-axis which are at the beginning and end of the vertical mode of motion in the z-axis. This may be attributed to the intensity values of the cells associated with their orientation change while exiting the vertical mode of motion and entering the planar mode of motion. Since the cell is aligned along the z-axis, the size of the cell is smaller than that of the cell when it moves in the xy plane. Since the mean value has been used, the intensity difference should increase because its size decreases.

The intensity difference, the size of the cell, and the eccentricity for the experiment are shown in Figure 7. The intensity difference between the cell and the background is greater when the cell is focused. In contrast, the intensity difference decreases when the cell moves away from the focal plane. From 0 to 8.5 seconds and 24.7 to 32.3 seconds, the cell travelled on the lower plane. Thus, the intensity difference is high and the size of the cell is small in Figure 7 (a). Since the cell is controlled in the upper plane between 10.7 and 22.3 seconds and after 34.8 seconds, the intensity difference is low and the size is larger. The fluctuation of the intensity difference when the cell moves in the lower plane is higher than that of the upper plane, while the variance of the z-axis position for both cases are similar at 19.0 and 19.4 μm for the lower and upper plane, respectively. Also, when the cell was controlled in planar mode, its fluctuation in the z-axis is also about 38 μm; this might be the minimum depth needed for *T. pyriformis* to swim freely. This fluctuation is due to the small position difference in the z-axis around the focal plane, creating a large intensity difference based on the fitted curve in Figure 5, in which the intensity difference decreases exponentially. When the cell is far from the focal plane, such as the upper plane, the fluctuation of intensity difference is not as pronounced, as expected from the lower slope in Figure 5.

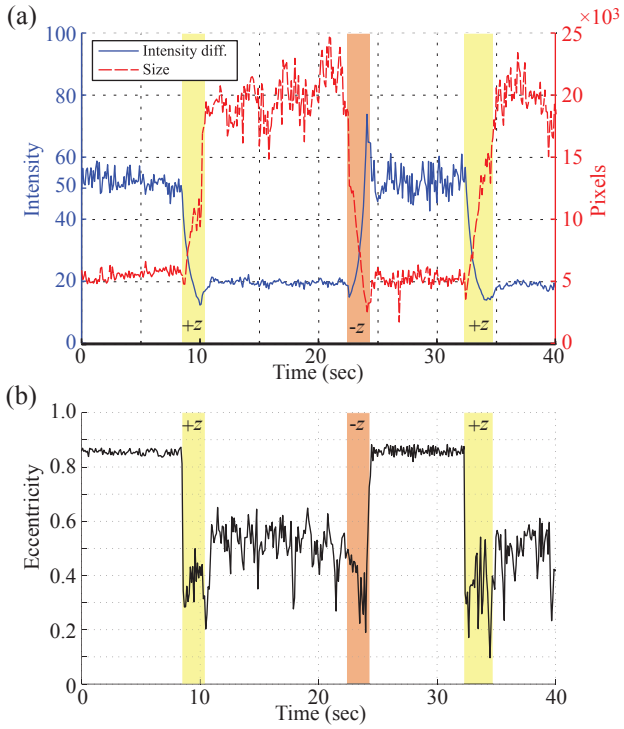

Fig. 7. (a) The intensity difference, size and (b) the eccentricity of the tracked cell. Light and dark yellow regions represent the period when positive and negative magnetic fields are applied along the z-axis, respectively

The size of the cell during the experiment is shown in Figure 7 (a). The average size of a normal cell is about 200 pixels. The lower plane is located over 100 μm above the focal plane; its size is about 600 pixels. When the cell moves on the upper plane, the size of cell is around 2000 pixels which is about 10 times larger than that of the cell on the focal plane. In contrast to the intensity difference, the fluctuation of a cell's size is small when the cell is close to the focal plane. In the upper plane, there is large variation of the cell size, possibly attributed to the poor intensity difference between the cell and the background. Even though the size has a relationship with the z-axis position, it is hard to use the size information to estimate the position in z-axis due to the large variance in cell size.

There are three trajectories in which the cell moves along the z-axis at 8.5 - 10.4, 22.4 - 24.3, and 32.3 - 34.7 seconds. The direction of the magnetic fields is indicated as '+z' and '-z' while electromagnets for the x and y axes are off. When the cell moves away from the focal plane, the intensity difference decreases and the size of the cell increases. Also, since the size decreases due to the cell's shape difference when it swims along the z-axis and on the xy plane, there are a decrease and an increase of the cell's area at the beginning and end of these durations, respectively, which might affect the localization in z-axis.

The eccentricity is the ratio of the distance between the foci of the ellipse to its major axis length. The eccentricity

is 0 for a circle and 1 for a line; *T. pyriformis* is considered as an ellipse. Thus, the eccentricity of a pear-shaped cell on the focal plane is normally around 0.8 - 0.9, as the average size of *T. pyriformis* is 25 μm by 50 μm [17]. Figure 7 (b) shows the eccentricity of the cell during the experiment. When the cell moves on the lower plane, which is close to the focal plane, the eccentricity is around 0.8569 with a variance 0.0128, which means the cell shape is maintained on the lower plane. However, the eccentricity decreased to around 0.5065 with a relatively large variance of 0.0807. Thus, it is verified that the cell shape on the image becomes more circular due to the blurred image. In addition, when the cell is controlled in vertical mode, the eccentricity decreased to around 0.4, indicating a more circular shape due only to the change in orientation. The eccentricity and the cell size may possibly be integrated with the intensity information for robust localization in the z-axis. The eccentricity may provide specific information as to whether the cell moves along the z-axis or not. While the cell swims close to the focal plane, the variance of the cell size is smaller than that of the intensity difference. When the cell size and intensity information is combined, the performance of cell localization would be enhanced.

V. CONCLUSIONS

In this paper, we have demonstrated three-dimensional control of a live organism, artificial magnetotactic *T. pyriformis*, as a microrobot and tracked its three-dimensional position using the intensity information of the cell. Artificial magnetotactic *T. pyriformis*, which internalizes iron oxide particles, was controlled by manipulating the swimming direction of a cell in three-dimensional space using two sets of Helmholtz coils and one coil for the z-axis. The locations in the z-axis were evaluated using the mean intensity of a cell which decreased exponentially above 20 μm from the focal plane. In addition, the changes of the size and eccentricity according to its depth are discussed. The three-dimensional control of magnetotactic *T. pyriformis* may be utilized for microscale engineering tasks such as target transport, cell therapy, and three-dimensional microassembly as a microrobot.

VI. ACKNOWLEDGMENTS

This work was funded by NSF CMMI Control Systems (award #1000284) and CBET Fluid Dynamics (award #0828167). We thank UKei Cheang and Yan Ou for their help.

REFERENCES

[1] A. Ghosh and P. Fischer, "Controlled Propulsion of Artificial Magnetic Nanostructured Propellers," *Nano Letters*, vol. 9, pp. 2243-2245, 2009.

[2] L. Zhang, *et al*., "Artificial bacterial flagella: Fabrication and magnetic control," *Applied Physics Letters*, vol. 94, p. 064107, 2009.

[3] L. Zhang, *et al*., "Micromanipulation using artificial bacterial flagella," in *Intelligent Robots and Systems, 2009. IROS 2009. IEEE/RSJ International Conference on*, 2009, pp. 1401-1406.

[4] Cheang, U.K., et al., Fabrication and magnetic control of bacteria-inspired robotic microswimmers.*Applied Physics Letters*, 2010 Vol. 97. 2010: p.213704.

[5] Kim, D.H., et al., Artificial magnetotactic motion control of *Tetrahymena pyriformis* using ferromagnetic nanoparticles: A tool for fabrication of microbiorobots. *Applied Physics Letters*, 2010. 97(17): p.173702.

[6] Kim, D.H., et al. Real-time feedback control using artificial magnetotaxis with rapidly-exploring random tree (RRT) for *Tetrahymena pyriformis* as a microbiorobot. in *Robotics and Automation, 2011. Proceedings. ICRA '11. IEEE International Conference on. 2011*. Shanghai, China.

[7] Berg, H.C., How to Track Bacteria. *Review of Scientific Instruments*, 1971. 42(6): p. 868-871.

[8] Drescher, K., K.C. Leptos, and R.E. Goldstein, How to track protists in three dimensions. *Review of Scientific Instruments*, 2009. Vol. 80. p. 014301.

[9] Thar, R., N. Blackburn, and M. Kuhl, A New System for Three-Dimensional Tracking of Motile Microorganisms. *Applied and Environmental Microbiology*, 2000. 66(5): p. 2238-2242.

[10] McMahon, M.D., et al., 3D Particle Trajectories Observed by Orthogonal Tracking Microscopy.*ACS Nano*, 2009. 3(3): p. 609-614.

[11] L. Köhidai and G. Csaba, "Effects of the mammalian vasoconstrictor peptide, endothelin-1, on *Tetrahymena pyriformis* GL, and the immunocytological detection of endogenous endothelin-like activity," *Comparative Biochemistry and Physiology Part C: Pharmacology, Toxicology and Endocrinology*, vol. 111, pp. 311-316, 1995.

[12] Kim, D.H., et al., Galvanotactic and phototactic control of *Tetrahymena pyriformis* as a microfluidic workhorse. *Applied Physics Letters*, 2009. 94(16): p. 163901.

[13] Lavin, D.P., et al., Size effects on the uptake of particles by populations of *Tetrahymena pyriformis* cells. *Journal of Eukaryotic Microbiology*, 1990. 37(3): p. 157-163.

[14] Kim, D.H., et al., Characterization of Deciliation-Regeneration Process of *Tetrahymena pyriformis* for Cellular Robot Fabrication. *Journal of Bionic Engineering*, 2011. 8(3): p. 273-279.

[15] J. William H. Hayt and J. A. Buck, *Engineering electromagnetics*, 7th edition ed. New York: McGraw-Hill, 2006.

[16] Cierpka, C., et al., On the calibration of astigmatism particle tracking velocimetry for microflows. *Measurement Science and Technology*, 2011. 22: p. 015401.

[17] Zilberg, D. and T. Sinai, Optimization and validation of a colorimetric assay for Tetrahymena sp. survival. *Research in Microbiology*, 2006. 157(4): p. 355-359.